LANGMUIR

Article

pubs.acs.org/Langmuir

Structured Nanoparticles from the Self-Assembly of Polymer Blends through Rapid Solvent Exchange

Nannan Li,[†] Athanassios Z. Panagiotopoulos,*[,†] and Arash Nikoubashman*[,‡]

[†]Department of Chemical and Biological Engineering, Princeton University, Princeton, New Jersey 08544, United States

[‡]Institute of Physics, Johannes Gutenberg University Mainz, Staudingerweg 7, 55128 Mainz, Germany

ABSTRACT: Molecular dynamics simulations were performed to study systematically the rapid mixing of a polymer blend in solution with a miscible nonsolvent. In agreement with experiments, we observe that polymers self-assemble into complex nanoparticles, such as Janus and core−shell particles, when the good solvent is displaced by the poor solvent. The emerging structures can be predicted on the basis of the surface tensions between the polymers as well as between the polymers and the surrounding liquid. Furthermore, the size of the nanoparticles can be independently tuned through the mixing rate and the polymer concentration in the feed stream; meanwhile, the composition of the nanoparticles can be controlled by the polymer feed ratio. Our results demonstrate that this process is highly promising for the production of structured nanoparticles in a continuous and scalable way with independent and precise control over particle size, morphology, and composition. Such tailored nanoparticles are highly sought after in various scientific and industrial applications, and our theoretical findings provide important guidelines for designing appropriate experimental fabrication processes.

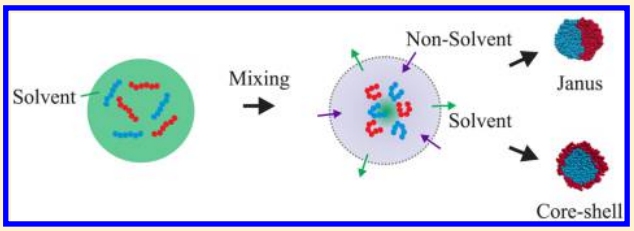

INTRODUCTION

Structured nanoparticles are important for many applications, including pharmaceuticals,[1,2] electronics,[3,4] and photonics.[5,6] Among various types of nanoscale structures, Janus and core−shell particles have attracted signficant attention; Janus nanoparticles, which are characterized by their two distinct domains, can be used as interfacial stabilizers and pigments in electronic paper,[7−9] whereas core−shell particles find applications in bioimaging and as carriers in drug delivery systems.[10] These applications require well-defined properties with narrow particle size and morphology distributions. However, these requirements pose a significant challenge for most existing manufacturing techniques. In addition, manufacturing techniques also need to be scalable to move beyond laboratory scales and to achieve commercially driven applications of these nanoparticles.

Various experimental methods have been developed for the fabrication of Janus or core−shell particles, such as seeded polymerization (lacks size and structure control),[11−13] templating (good size and shape control but involves multiple manual steps),[14,15] particle lithography (allows coating of particles but is limited by scale-up issues),[16,17] synthesis in microfluidic reactors (can scale up and operate in a continuous fashion, but the particle size distribution is wide and morphology control is difficult),[18−20] and internal phase separation, e.g., the self-organized precipitation (SORP) method[21] and miniemulsion polymerization.[22] In particular, the SORP method has demonstrated the ability to produce Janus and core−shell particles from different combinations of homopolymers depending on their solubilities in the poor solvent, and the relation has also been confirmed by a computational study using dissipative particle dynamics simulations.[23] The SORP method has also been applied to block copolymers, for which morphologies including lamellar and onionlike structures were formed.[24−26] However, most of the aforementioned processes involve batch processing steps, and the fabricated nanoparticles cannot always be readily available with high accuracy. It is thus clear that further research is required to develop fabrication methods that are both scalable and allow for precise control over particle size, morphology, and composition.[27,28]

The present work has been motivated by a novel experimental approach for creating structured particles, namely, flash nanoprecipitation (FNP),[29,30] where a polymer solution is rapidly mixed with an excess amount of a nonsolvent to induce aggregation into nanoparticles. Compared to other competing methods, FNP stands out as a one-step continuous process that operates at room temperature, consumes little energy, and has scale-up potential. Previously, FNP was used to embed small hydrophobic drug molecules into nanoparticles, stabilized via amphihilic block copolymers,[31−34] as well as to produce homopolymer nanoparticles.[35,36] Recently, it has been experimentally demonstrated that the FNP technique can be used to produce Janus and multifaced nanoparticles from blends of commercially available homopolymers.[37,38] Most importantly, the process was shown to provide precise and independent control over particle size, morphology, and composition.

Received: January 26, 2017
Revised: March 10, 2017
Published: March 17, 2017

DOI: 10.1021/acs.langmuir.7b00291
Langmuir 2017, 33, 6021−6028

The underlying microscopic mechanisms responsible for the self-assembly are still elusive because the FNP process takes place on nanometer length scales and millisecond time scales, which makes the experimental study of this process difficult. Furthermore, it is an expensive and time-consuming task to systematically search and screen in the experiments all relevant process parameters, such as the feed ratio, feed concentration, flow rate, and molecular properties. Computer simulations can provide considerably more microscopic-level information than experiments and are therefore useful tools in the study of complex mechanisms and morphologies. They also offer advantages in efficient parameter space searching. Previous efforts have focused on the self-assembly of polymer-protected nanoparticles[33,34] and neutral homopolymers in FNP,[36] and the current study expands previous models to account for polymer blends.

In the present work, molecular dynamics (MD) simulations are performed to explore systematically how different processing parameters in FNP such as the hydrophobicity and chemical compatibility of the polymers, mixing rate, polymer feed concentration, and ratio affect the size and morphology of the precipitated nanoparticles. The structure of this article is as follows: we will first summarize the MD simulation model and methods used in the present work. Next, we present and analyze our simulation results, focusing on how the particle morphology, size, and composition can be independently tuned by the aforementioned parameters. Finally, we summarize our results and comment on the future directions we will take to study nanoparticle production from the FNP process.

SIMULATION MODEL AND METHODS

Our previous MD model for homopolymers undergoing the FNP process serves as a foundation for our study of polymer blends.[36] In this model, a polymer is described as a linear bead−spring chain with N beads, each with unit diameter σ and mass m. Each bead represents a Kuhn segment of the polymer chain. In the experiments, the polystyrene (PS) chains have a molecular weight of 16.5 kg/mol.[37] Because the mass of a PS Kuhn segment is M_k = 0.72 kg/mol,[39] we obtained N = 23, which was used for all homopolymer chains in our simulations.

The bonded interactions between polymer beads are modeled via the finitely extensible nonlinear elastic (FENE) potential.[40] The standard Kremer−Grest parameters were adopted to prevent unphysical bond crossing.[41] Other than the bonded interactions, polymer beads also interact with one another via the standard Lennard-Jones (LJ) potential

$$U_{LJ}(r_{ij}) = 4\varepsilon_{LJ}\left[\left(\frac{\sigma}{r_{ij}}\right)^{12} - \left(\frac{\sigma}{r_{ij}}\right)^{6}\right] \quad (1)$$

with r_{ij} being the interparticle distance between beads i and j. Binary polymer blends have been considered in the current work, and we set the prefactor ε_{LJ} for the intraspecies interactions of both polymer A and polymer B equal such that $\varepsilon_{AA} = \varepsilon_{BB} = k_BT$, with Boltzmann constant k_B and temperature T. The interspecies AB interaction strength, ε_{AB}, was varied between $0.9\varepsilon_{AA}$ and $0.01\varepsilon_{AA}$ to mimic the chemical incompatibility of the two polymer types. The cutoff radius was set to $r_{cut} = 3.0\sigma$.

Following ref 36, solvent particles are modeled explicitly as LJ particles with the same size and mass as the polymer beads. A reduced number density of ρ_S = 0.66 has been chosen, which leads to a dynamic solvent viscosity of η = 1.01. Similar to previous computational studies on FNP,[33,34,36] nonbonded interactions on all particles were varied simultaneously over a certain period of time, τ_{mix}, to mimic the transition from good to poor solvent conditions. In our studies, we control the interaction between solvent particles and monomers by a dimensionless parameter λ[42]

$$U_{MS}(r_{ij}) = \lambda U_{WCA}(r_{ij}) + (1 - \lambda)U_{LJ}(r_{ij}) \quad (2)$$

where $U_{WCA}(r_{ij})$ is the purely repulsive Weeks−Chandler−Anderson (WCA) potential.[43] As λ increases from 0 to 1, the solvent quality changes from good to poor.

To make meaningful comparisons between our simulations and experimental results, it is important to establish a connection among units of energy, length, and time in the two domains, which has been done in ref 36 for the homopolymer−solvent model. The experiments were performed at room temperature T_{room} = 298 K, and thus $\varepsilon = k_BT_{room} = 4.11 \times 10^{-21}$ J for the characteristic energy. For the length scale, the radius of gyration of a single polymer chain in a Θ solvent, $R_{g,\Theta} = 2.35\sigma$, was compared to $R_{g,\Theta}$ of the corresponding PS chain (3.5 nm), leading to σ = 1.5 nm. For the time scale, the diffusion coefficient of a polymer chain under good solvent conditions, i.e., λ = 0, was compared to the experimental diffusion coefficient of a PS chain (extrapolated to the same molecular weight as in the simulations) in THF at room temperature (1.4×10^{-6} cm^2/s),[44] which led to a time conversion factor of τ = 0.28 ns.

During the FNP process, the polymer chains aggregate to nanoparticles in order to minimize the contact surface with the surrounding poor solvent. Without a stabilizing mechanism, all polymers eventually form a single aggregate because this configuration provides the lowest surface tension. However, in our case, nanoparticle stability is provided by a negative surface potential of between −30 and −40 mV, which was measured experimentally on particles of radii between 45 and 135 nm using electrophoretic light scattering.[36] Therefore, in addition to the bonded and nonbonded potentials between polymer beads, we also included a surface potential of ζ = −33 mV on the nanoparticles. This effect was mimicked by placing a virtual particle at the center of each aggregate, which carried the equivalent surface charge. Electrostatic interactions are switched off under good solvent conditions (ζ = 0 mV). As the solvent quality worsens, the buildup of surface charges is mimicked by linearly decreasing ζ to its final value (ζ = −33 mV). In our previous work,[36] we found that the precipitated nanoparticles became smaller as the ζ potential became more negative, whereas pH had only a minimal effect on the final aggregate size. More details on this method can be found in prior work by Nikoubashman et al.[36]

The MD simulations were run using the HOOMD simulation package.[45,46] A cubic box with an edge length of 80σ, containing 337 920 solvent particles and a total of up to 1024 polymers at various A/B ratios was adopted. We have checked the influence of box size on the simulation results at selected state points and did not find any appreciable finite size effects when the box edge length is above 80σ. It is noted that the total number of 1024 polymers in our systems limits the maximum nanoparticle radius to $a \approx 21$ nm, which is 1 order of magnitude smaller than those produced in the experiments. To realize in the simulations a nanoparticle with a radius of a = 100 nm, approximately 10^5 polymers are required, which is computationally unfeasible. Despite this limitation, however, the model is able to reproduce the most important trends observed in the experiments.[36] A Nosé−Hoover thermostat was employed to maintain the temperature at T = 1, and the equations of motion were integrated using the velocity Verlet algorithm at a time step of Δt = 0.01 in the reduced units defined earlier.

RESULTS AND DISCUSSION

Torza and Mason investigated the equilibrium morphology of droplets in systems consisting of three immiscible liquids using the Neumann triangle.[47] Depending on the values of the surface tensions, core−shell, acorn-shaped, or separated droplets were obtained. These predictions were based on theoretical calculations on macroscopic systems, and it is not immediately clear whether these considerations are directly

DOI: 10.1021/acs.langmuir.7b00291
Langmuir 2017, 33, 6021−6028

transferable to the nanoscale systems at hand. Subsequent studies have also used surface tension to interpret the phase-separated structures of polymer blends in aqueous solutions.[23,48−52] Therefore, to understand the different particle morphologies produced from the FNP process, we first determined the surface tension between our constituents. To this end, we performed simulations on systems consisting of two homopolymer slabs as well as a homopolymer slab surrounded by solvent particles at $T = 1$. Surface tension values between the two polymers and between polymers and the solvent were calculated using the standard mechanical definition[53]

$$\gamma = \frac{L_z}{2}\left\langle P_{zz} - \frac{P_{xx} + P_{yy}}{2} \right\rangle \tag{3}$$

where L_z is the length of the simulation box along the z axis, which was allowed to vary. P_{xx}, P_{yy}, and P_{zz} are the diagonal components of the pressure tensor along the x, y, and z axes, respectively, and the brackets denote an ensemble average.

As seen in Figure 1, the polymer−polymer surface tension, γ_{AB}, decreases with increasing ε_{AB} and vanishes as expected

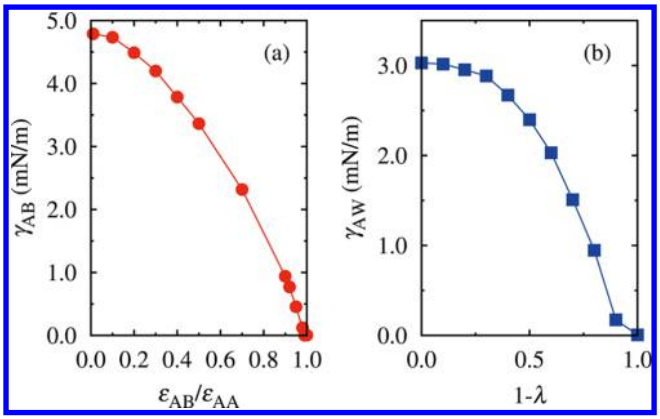

Figure 1. (a) Polymer−polymer surface tension, γ_{AB}, as a function of the reduced polymer cross interactions, $\varepsilon_{AB}/\varepsilon_{AA}$ ($\varepsilon_{AA} = \varepsilon_{BB}$). $\varepsilon_{AB}/\varepsilon_{AA}$ was varied between 0.01 to 1.0. (b) Polymer−solvent surface tension, γ_{AW}, as a function of the solvent quality parameter, $1 - \lambda$.

when ε_{AB} becomes identical to ε_{AA} and ε_{BB}. Meanwhile, the polymer−solvent surface tension, γ_{AW}, decreases when the polymer−solvent interaction becomes less repulsive and reaches 0 when $1 - \lambda = 1$, i.e., when the polymer−solvent interaction is purely LJ. Our calculated surface tensions are comparable to those of real systems, e.g., $\gamma_{PS,PMMA} = 3.2$ mN/m and $\gamma_{PS,water} = 15.0$ mN/m,[49,50,52] when the conversions described earlier from experimental to simulation energy and length scales are used. Because our coarse-grained model was not parametrized using surface tensions of specific polymers and solvents, e.g., PS and THF, the calculated values are not expected to agree perfectly with experimental measurements. However, as will be shown in Figure 2, the phase behavior of the polymer blends is predominantly dictated by the *ratio* of surface tensions and not their absolute values. In this respect, our model produces quantitatively similar values for γ_{AW}/γ_{AB} and γ_{BW}/γ_{AB} as for typical materials in experiments.

Having obtained the surface tensions of the polymer blend and solvent systems, we used Torza and Mason's criteria[47] to explain the different particle morphologies from FNP. Here, we adopted the phase diagram reported in ref 52 to draw the solid

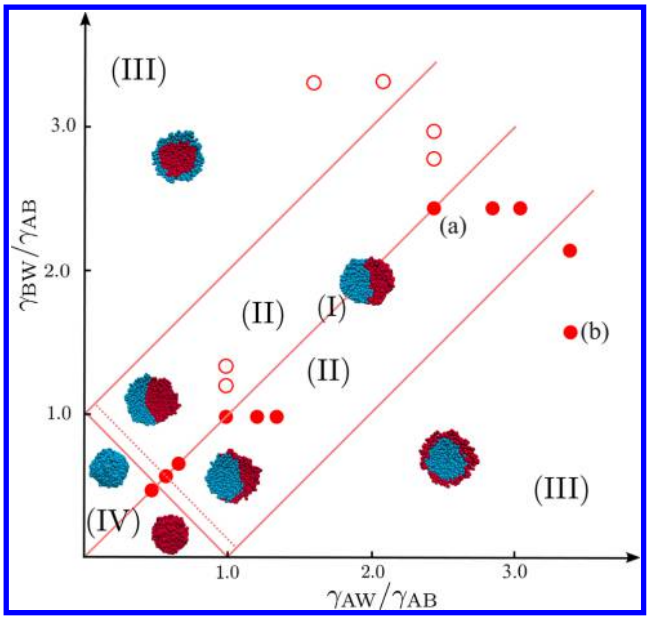

Figure 2. Equilibrium morphologies of nanoparticles as a function of the ratios of surface tensions. Solid lines are reproduced from ref 52 and they are based on predictions by Torza and Mason using the Neumann triangle.[47] The positions of the lines are verified by our analysis of an isolated nanoparticle. Cross sections of Janus and core−shell particles (region I−III) are shown here to reveal the internal structure. The dashed line represents the boundary between regions II and IV if a negative surface potential of $\zeta = -33$ mV is applied. Closed circles are state points examined in our MD simulations on FNP systems at $\tau_{mix} = 21$ μs. Open circles are symmetrical state points. Points (a) and (b) are chosen from the Janus and core−shell regions for studies on particle size and composition, as will be explained later.

lines in Figure 2. State points highlighted by the closed circles have been examined in our simulations on FNP systems at $\tau_{mix} = 21$ μs, and because $\varepsilon_{AA} = \varepsilon_{BB}$, symmetrical state points have also been labeled by the open circles. We obtained particle morphologies consistent with predictions from Torza and Mason's criteria, i.e., dumbbell-shaped Janus particles in region I, acorn-shaped Janus particles in region II, core−shell particles in region III, and completely phase-separated aggregates in region IV. However, it is noted that when a negative surface potential was applied to mimic the effect of charge stabilization during FNP, the boundary between regions II and IV shifted slightly upward as represented by the dashed line. The positions of the lines drawn in Figure 2 will be further studied by our analysis of an isolated nanoparticle (see ensuing discussion).

To differentiate the assembly mechanisms that lead to different particle morphologies, we present simulation snapshots for both the Janus and core−shell particles in Figure 3. In case (a), when the difference in the solvophobicity of A and B was small, polymers A and B formed separate aggregates first, and the homogeneous aggregates merged to form Janus particles as mixing proceeded. When the difference in the solvophobicity of A and B was large as in case (b), the more solvophobic polymers aggregated first and the less solvophobic polymers then spread out on the surface of the aggregates to form core−shell particles.

Next, we examined the self-assembled Janus and core−shell structures in more detail. We obtained an isolated Janus particle (the middle nanoparticle structure in Figure 4) with 93 A chains and 93 B chains from a simulation with $\varepsilon_{AB} = 0.9\varepsilon_{AA}$ and

DOI: 10.1021/acs.langmuir.7b00291
Langmuir 2017, 33, 6021−6028

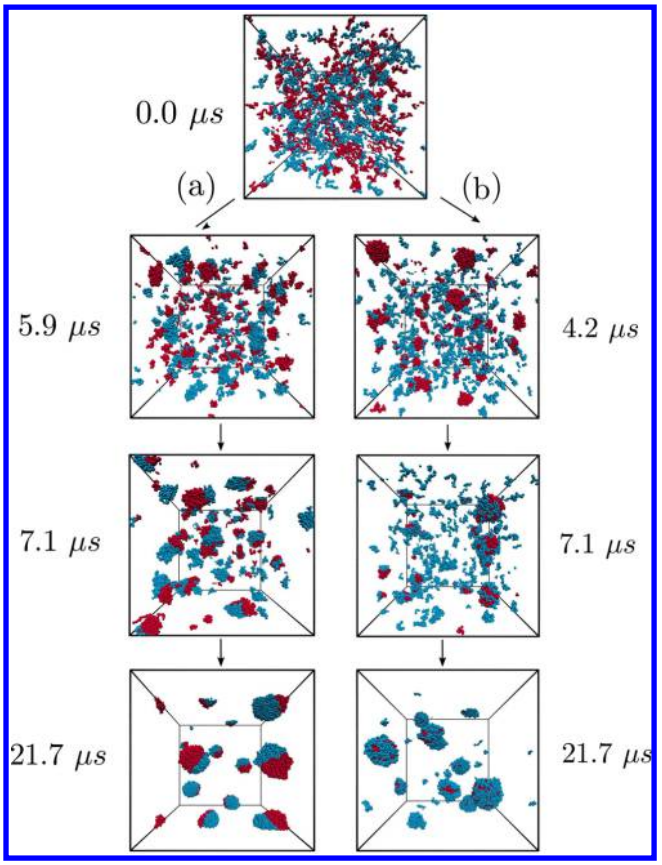

Figure 3. Simulation snapshots over time that represent two selected assembly parameters for a polymer blend undergoing the FNP process with τ_{mix} = 21 μs. Case (a) leads to the formation of Janus particles, and case (b) leads to core−shell particles.

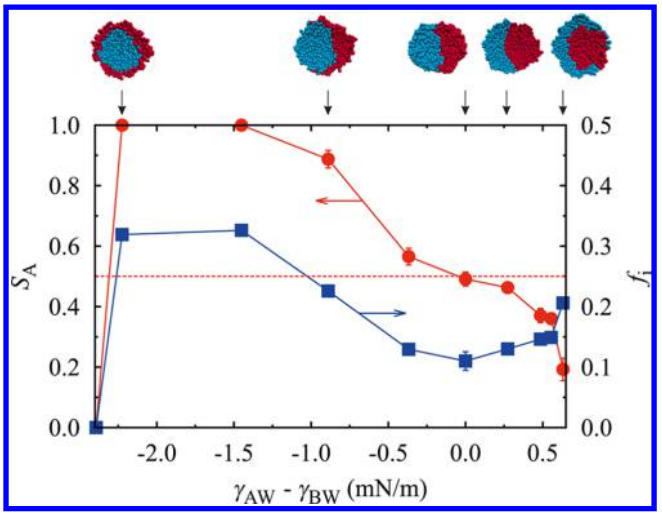

Figure 4. Surface coverage of polymer A, S_A, and the fraction of beads that belong to the A−B interface, f_i, as a function of $\gamma_{AW} - \gamma_{BW}$.

$\lambda_{AW} = \lambda_{BW} = 0.5$ and studied how the structure changed as we varied polymer−solvent and polymer−polymer interactions. We first kept ε_{AB} and λ_{BW} constant (γ_{AB} = 0.9 mN/m and γ_{BW} = 2.4 mN/m). By varying λ_{AW} systematically from 0 to 1, which can be represented by a horizontal move from left to right across Figure 2, we observed particle structures as shown in Figure 4. Here, two structural properties were used to characterize the varying degree of encapsulation, i.e., the surface coverage of A-type beads, S_A, and the fraction of beads that belong to the A−B interface, f_i. Quantity S_A was obtained by identifying and constructing the convex hull of the surface beads. To calculate f_i, we first identified the A−B interface by taking all of the beads that have at least one bead of an opposite type in their immediate neighborhood, and then dividing this number by the total number of beads in the particle.

As shown in Figure 4, S_A increases as λ_{AW} decreases, which results from an increasing degree of encapsulation by A. The dashed line at S_A = 0.5 is the predicted surface coverage by assuming that the area scales as the power of 2/3 of the number of beads; this line intersects the data at $\gamma_{AW} - \gamma_{BW}$ = 0 mN/m, when the nanoparticle is dumbbell-shaped with no encapsulation. At $\gamma_{AW} - \gamma_{BW}$ = −0.94 mN/m as predicted by the lines drawn between regions II and III in Figure 2, the particle undergoes a transition from Janus to core−shell, which is in agreement with the measurements presented in Figure 4. Finally, when $\gamma_{AW} - \gamma_{BW}$ = −2.4 mN/m, i.e., γ_{AW} = 0 mN/m, polymer chains of type A dissolve in the solvent. It is also clear that calculations of f_i support the same observations.

Next, we fixed both λ_{AW} and λ_{BW} at 0.5 and decreased ε_{AB} from 0.9 to 0.01. In addition to f_i, we also computed the asphericity of a single Janus particle, α.[54] The quantity α characterizes the shape of the particle and is defined by

$$\alpha = \frac{(L_1^2 - L_2^2)^2 + (L_1^2 - L_3^2)^2 + (L_2^2 - L_3^2)^2}{2(L_1^2 + L_2^2 + L_3)^2} \quad (4)$$

where L_1, L_2, and L_3 are the eigenvalues of the particle's radius of gyration tensor. The shape of the particle is a sphere when α = 0.

As shown in Figure 5, the dumbbell-shaped Janus particle became more elongated with a decreasing interfacial area. In the absence of the negative surface potential, at $\varepsilon_{AB} = 0.01\varepsilon_{AA}$, which corresponds to a γ_{AB} value of 4.8 mN/m, the Janus particle separates into two homopolymer aggregates (not shown in Figure 5), which is in agreement with Torza and Mason's prediction, and the solid line drawn between regions II and region IV in Figure 2. When a negative surface potential of ζ = −33 mV is applied, the separation occurs at $\varepsilon_{AB} = 0.3\varepsilon_{AA}$ which corresponds to γ_{AB} = 4.2 mN/m and $\gamma_{AW}/\gamma_{AB} = \gamma_{BW}/\gamma_{AB}$ = 0.57, leading to the dashed line drawn in Figure 2.

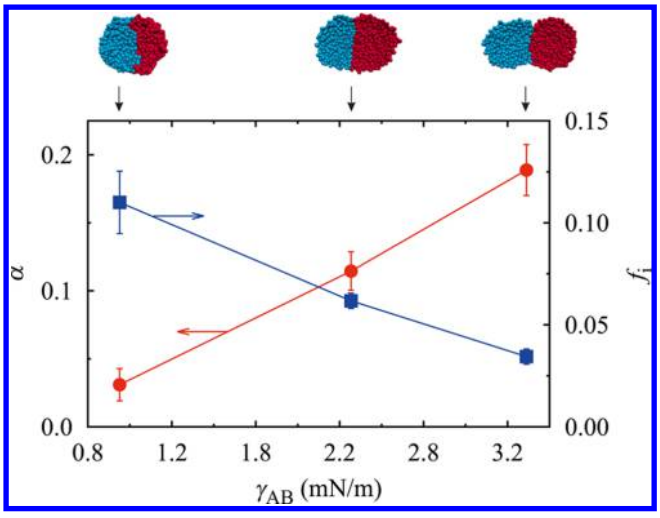

Figure 5. Asphericity, α, and the fraction of beads that belong to the A−B interface, f_i, as a function of γ_{AB}.

DOI: 10.1021/acs.langmuir.7b00291
Langmuir 2017, 33, 6021−6028

Having understood the relationship between particle structure and surface tension, we moved on to study the processing parameters specific to the FNP process, such as the mixing rate and polymer feed concentration. An advantage of the FNP technique is the ability to independently control the particle size and morphology, as demonstrated by recent experiments in which the size of the patchy particles was tuned by the mixing rate or polymer feed concentration.[37] In the following section, we will present results from varying these two parameters in our simulations.

Two state points have been chosen from the phase diagram [(a) and (b) in Figure 2], which belong to the Janus and core−shell regions, respectively. It has been suggested by the experiments and previous simulations of homopolymers that the particle size remains approximately constant at short mixing times, i.e., fast mixing, but increases when the mixing time exceeds a specific threshold.[36,37] It was argued that micromixing affects only the final nanoparticle size when the collapse time of polymer chains during the solvent displacement is slower than the average contact time for two polymer chains. Reference 36 provides details on estimating the average contact time and thus the threshold mixing time, which has been indicated by the dashed line in Figure 6 for the studied system. Figure 6 also

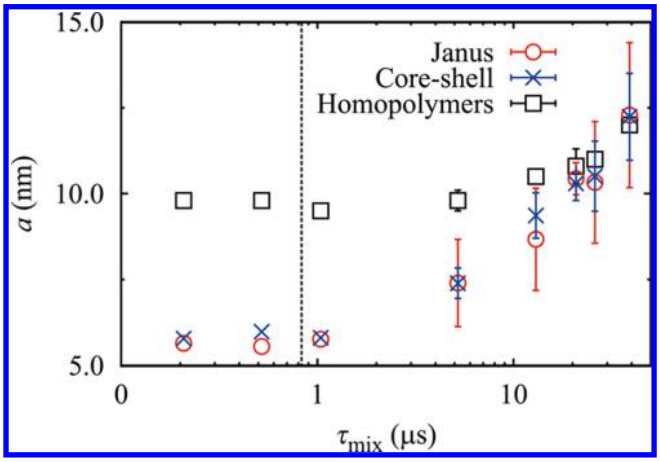

Figure 6. Average radius of nanoparticles (Janus, core−shell, and homopolymers), a, plotted as a function of mixing time, τ_{mix}. The dashed line indicates the estimated threshold mixing time for the homopolymers at the studied concentration of 8.2 mg/mL. Error bars are shown only when they are larger than the symbol size.

shows the average size of Janus and core−shell particles as a function of τ_{mix}, and it is clear that polymer blends exhibit a trend similar to that of homopolymer systems. Interestingly, at fast mixing, precipitated Janus or core−shell particles are smaller than their homopolymer counterparts ($\varepsilon_{AA} = \varepsilon_{BB} = \varepsilon_{AB}$) at the same overall polymer concentration. This discrepancy stems from $\varepsilon_{AB} < \varepsilon_{AA} = \varepsilon_{BB}$ in our simulations, which leads to a smaller enthalpic gain when polymers of different types aggregate. This effect vanishes, however, at longer τ_{mix}, and the particle diameters approach each other, despite the slightly unfavorable ε_{AB}; at such long mixing times, the polymers have enough time to aggregate before the good solvent is displaced by the poor one and the stabilizing surface charge builds up. Recent self-consistent field theory calculations of a similar system have indicated that $a \approx \tau_{mix}^{1/6}$ in this growth regime,[55] which is in line with our observations.

Unlike systems of homopolymers undergoing FNP, τ_{mix} not only affects the final particle size in the case of polymer blends but also leads to different compositions of the final system at equilibrium. During Janus particle formation, at fast mixing, a certain fraction of precipitated nanoparticles remains as homopolymer aggregates as shown in Figure 7. As τ_{mix}

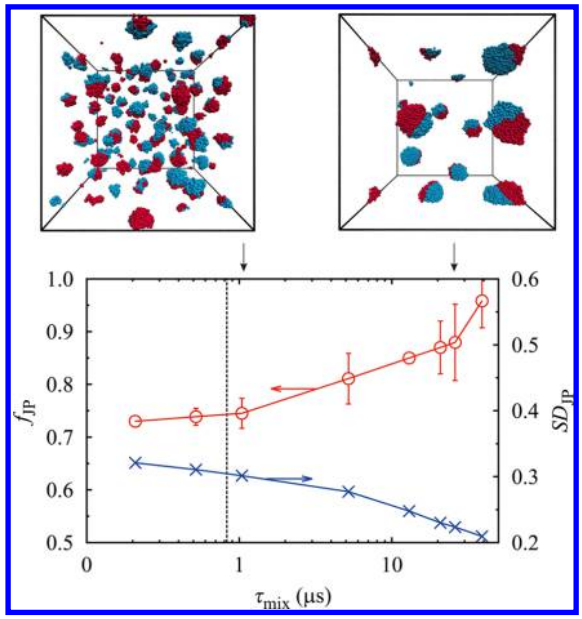

Figure 7. Fraction of Janus particles, f_{JP}, and the standard deviation from a 50:50 A/B ratio in the precipitated particles, SD_{JP}, plotted as a function of mixing time, τ_{mix}. The dashed line indicates the estimated threshold mixing time for the homopolymers at the studied concentration of 8.2 mg/mL.

increases, the fraction of Janus particles, f_{JP}, increases and approaches 1. Figure 7 also shows the standard deviation of nanoparticle compositions from a 50:50 A/B ratio, SD_{JP}. As τ_{mix} increases, SD_{JP} decreases as a result of the longer diffusion and aggregation time allowed before charge stabilization sets in.

The effect of mixing time on the final systems of core−shell particles has also been examined. As shown in Figure 8, at small τ_{mix}, a large fraction of the less solvophobic chains remain dissolved in the solvent. Therefore, the average composition of A chains in the precipitated nanoparticles, f_A, deviates from 0.5, and the amount of surface coverage by A particles, S_A, is significantly larger than zero because the core is not completely covered by the less solvophobic B chains. However, as τ_{mix} increases, the number of free chains in the final system decreases, and f_A and S_A approach 0.5 and 0, respectively. It should also be noted that the number of dissolved less solvophobic chains could be overestimated in our simulations because they were assigned a larger artificial charge as a result of their large radius of gyration; although the origin of the negative surface potential is still unclear,[56−58] it is conceivable that only highly hydrophobic, collapsed aggregates carry such a surface potential. However, the general trends in our observations and the studied metrics should still hold as demonstrated through the analysis of the single isolated aggregates, where the surface charge was switched off. In addition, it can be seen in Figures 7 and 8 that the studied metrics remain relatively constant at short mixing time and start to vary more prominently after a threshold value. This observation can be understood with the concept of the

DOI: 10.1021/acs.langmuir.7b00291
Langmuir 2017, 33, 6021−6028

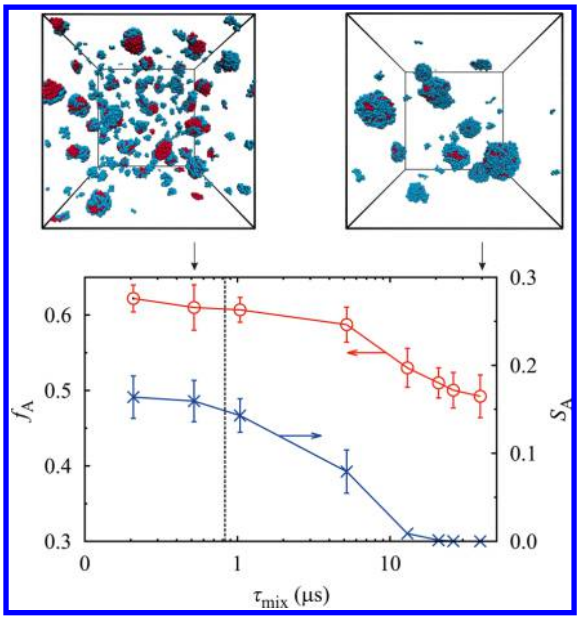

Figure 8. Average composition of A chains, f_A, and the amount of surface coverage of A particles in the precipitated particles, S_A, plotted as a function of mixing time, τ_{mix}. The dashed line indicates the estimated threshold mixing time for the homopolymers at the studied concentration of 8.2 mg/mL.

aforementioned threshold mixing time, which has been used to explain the trend in final nanoparticle size in Figure 6.

In addition to τ_{mix}, we have also studied the effect of polymer feed concentration, Φ, on the average nanoparticle radius, a, as shown in Figure 9. We obtained good agreement with results

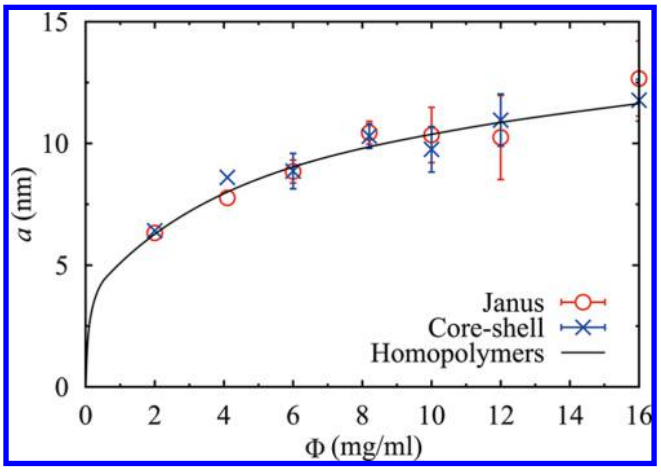

Figure 9. Nanoparticle radius a vs overall polymer concentration in the mixed stream Φ at τ_{mix} = 21 μs.

from previous MD simulations on homopolymers for τ_{mix} = 21 μs. The data can be fitted through $a \propto \Phi^n$ with $n \approx 0.3$ as in the experiments.[36] The fact that nanoparticle size increases with polymer feed concentration confirms that the process is growth-controlled, which fundamentally differs from a nucleation-controlled process, where the final nanoparticle size was found to decrease with polymer concentration because polymers deposit on a larger number of nuclei that are formed.[35] In our previous work, we studied the size distribution of the precipitated nanoparticles for homopolymeric systems via experiments and simulations, and we found normal size distributions with polydispersity indices of approximately 0.1.[36] We did not make such a quantitative analysis of the size distribution in the case of polymer blends because of the small number of samples, but a visual inspection revealed behavior that was qualitatively similar to that in the homopolymer case.

Finally, we investigated the effects of the polymer feed ratio on the final nanoparticle composition profile at τ_{mix} = 21 μs and Φ = 8.2 mg/mL. Three different A/B feed ratios, i.e. 1:1, 1:2, and 1:4, were studied for both the Janus and the core−shell regimes. It was found that feed ratio, $f_{A,feed}$, had no effect on the nanoparticle size. At long mixing time, the average composition of A in precipitated nanoparticles at equilibrium, $f_{A,particle}$, converged to $f_{A,feed}$ as shown in Figure 10. This is because the

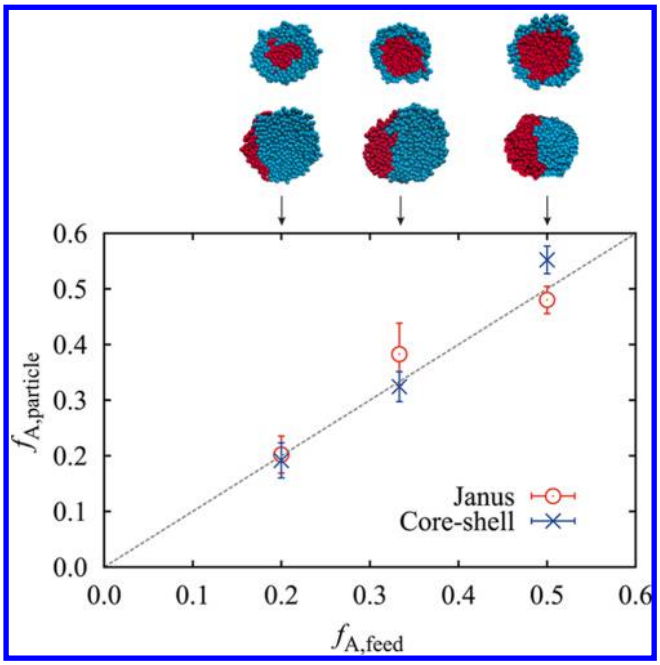

Figure 10. Average fraction of polymer A in equilibrium particles, $f_{A,particle}$, as a function of the fraction of polymer A in the feed stream, $f_{A,feed}$ at τ_{mix} = 21 μs. The dashed line represents $f_{A,particle} = f_{A,feed}$. Examples of particle cross sections from each feed ratio are also shown.

polymers are homogeneously distributed, and when they are allowed a long enough time to aggregate before the good solvent is displaced by the poor one, the compositions of individual nanoparticles should approach that of the feed stream. In experiments, τ_{mix} is typically on the order of milliseconds, which is 1 to 2 orders of magnitude larger than the τ_{mix} studied in our simulations. The experimentally studied polymer concentrations range from 0.1 to 2 mg/mL, which is 1 order of magnitude lower than the polymer concentration range studied by our simulations. At such lower concentrations in the experiments, the threshold mixing time is raised by approximately a factor of 5 to ∼5 μs, which is still well below the characteristic mixing time of ∼3 ms. Hence, the effect of a lower polymer concentration can still be offset by the much larger τ_{mix}, and nanoparticles produced in the experiments should belong to the regime where their compositions converge to the feed composition, which is consistent with experimental observations.[37] Therefore, we can conclude that the FNP technique can reliably control the composition of the fabricated nanoparticles through the polymer feed ratio.

DOI: 10.1021/acs.langmuir.7b00291
Langmuir 2017, 33, 6021−6028

CONCLUSIONS

In this work, MD simulations have been carried out to systematically explore how polymer−polymer and polymer−solvent surface tensions control the internal structures of nanoparticles (Janus and core−shell) produced from the FNP process. It was found that the final equilibrium structure can be predicted by the surface tensions between the polymer blend and between the polymers and the solvent, which qualitatively agree with previous experimental and computational studies on phase-separated structures of polymer blends in aqueous solutions.[23,48−52]

We have also demonstrated the ability of the FNP process to independently tune the particle size through the mixing time of the solvent−nonsolvent streams and the overall polymer concentration as well as the particle composition through the polymer feed ratio. Our simulations show that the particle size remains relatively constant for fast mixing and increases with mixing time beyond a certain threshold time as well as the overall polymer concentration in the feed stream. The above relations agree with the experimental results and MD simulations on homopolymer systems.[36,37] The average particle composition was also found to approach the feed ratio at long mixing time. Finally, we were also able to elucidate the mechanism of Janus or core−shell particle formation in our simulations; i.e., the homopolymers form separate aggregates before they merge to form structured particles.

The experimental technique and the generic simulation model should be generally applicable to many other polymer blend systems undergoing rapid solvent exchange. We have thus demonstrated FNP as a simple, continuous, and scalable process to produce structured nanoparticles with nanoscale control. Our results also provide guidelines for the future design and preparation of polymeric nanoparticles with desired properties using FNP techiniques and thus facilitate their applications in areas such as drug delivery, sensors, and emulsion stabilization. Our future work will be concerned with accounting for the vitrification of the precipitated polymers because recent experiments[37] suggested that this effect might lead to multifaced nanoparticles.

AUTHOR INFORMATION

Corresponding Authors

*E-mail: azp@princeton.edu.
*E-mail: anikouba@uni-mainz.de.

ORCID

Athanassios Z. Panagiotopoulos: 0000-0002-8152-6615
Arash Nikoubashman: 0000-0003-0563-825X

Notes

The authors declare no competing financial interest.

ACKNOWLEDGMENTS

Financial support for this work was provided by the Princeton Center for Complex Materials (PCCM), a U.S. National Science Foundation Materials Research Science and Engineering Center (grant DMR-1420541). Furthermore, N.L. acknowledges funding from the Agency for Science, Technology and Research (A*STAR), Singapore. A.N. acknowledges funding from the German Research Foundation (DFG) under project number NI 1487/2-1.

REFERENCES

(1) Langer, R.; Tirrell, D. A. Designing materials for biology and medicine. *Nature* **2004**, *428*, 487−492.
(2) Champion, J. A.; Katare, Y. K.; Mitragotri, S. Designing Materials for Biology and Medicine. *Proc. Natl. Acad. Sci. U. S. A.* **2007**, *104*, 11901−11904.
(3) Liddell, C. M.; Summers, C. J.; Gokhale, A. M. Stereological Estimation of the Morphology Distribution of ZnS Clusters for Photonic Crystal Applications. *Mater. Charact.* **2003**, *50*, 69−79.
(4) Wang, X.; Summers, C. J.; Wang, Z. L. Large-Scale Hexagonal-Patterned Growth of Aligned ZnO Nanorods for Nano-optoelectronics and Nanosensor Arrays. *Nano Lett.* **2004**, *4*, 423−426.
(5) Fudouzi, H.; Xia, Y. Photonic Papers and Inks: Color Writing with Colorless Materials. *Adv. Mater.* **2003**, *15*, 892−896.
(6) Gratzel, M. Photoelectrochemical Cells. *Nature* **2001**, *414*, 338−344.
(7) Walther, A.; Matussek, K.; Müller, A. H. E. Engineering Nanostructured Polymer Blends with Controlled Nanoparticle Location using Janus Particles. *ACS Nano* **2008**, *2*, 1167−1178.
(8) Comiskey, B.; Albert, J. D.; Yoshizawa, H.; Jacobson, J. An Electrophoretic Ink for All-Printed Reflective Electronic Displays. *Nature* **1998**, *394*, 253−255.
(9) Nisisako, T.; Torii, T.; Takahashi, T.; Takizawa, Y. Synthesis of Monodisperse Bicolored Janus Particles with Electrical Anisotropy Using a Microfluidic Co-Flow System. *Adv. Mater.* **2006**, *18*, 1152−1156.
(10) Kwon, G. S.; Kataoka, K. Block Copolymer Micelles as Long-Circulating Drug Vehicles. *Adv. Drug Delivery Rev.* **1995**, *16*, 295−309.
(11) Chen, Y.; Dimonie, V.; El-Aasser, M. S. Effect of Interfacial Phenomena on the Development of Particle Morphology in a Polymer Latex System. *Macromolecules* **1991**, *24*, 3779−3787.
(12) Okubo, M.; Izumi, J.; Hosotani, T.; Yamashita, T. Production of Micron-Sized Monodispersed Core/Shell Polymethyl Methacrylate/Polystyrene Particles by Seeded Dispersion Polymerization. *Colloid Polym. Sci.* **1997**, *275*, 797−801.
(13) Lee, J.; Yezer, B. A.; Prieve, D. C.; Behrens, S. H. Janus Particles in a Nonpolar Solvent. *Langmuir* **2016**, *32*, 3095−3099.
(14) Cui, J. Q.; Kretzschmarr, I. Surface-Anisotropic Polystyrene Spheres by Electroless Deposition. *Langmuir* **2006**, *22*, 8281−8284.
(15) Boker, A.; He, J.; Emrick, T.; Russell, T. P. Self-Assembly of Nanoparticles at Interfaces. *Soft Matter* **2007**, *3*, 1231−1248.
(16) Snyder, C. E.; Yake, A. M.; Feick, J. D.; Velegol, D. Nanoscale Functionalization and Site-Specific Assembly of Colloids by Particle Lithography. *Langmuir* **2005**, *21*, 4813−4815.
(17) Yake, A. M.; Snyder, C. E.; Velegol, D. Site-Specific Functionalization on Individual Colloids:? Size Control, Stability, and Multilayers. *Langmuir* **2007**, *23*, 9069−9075.
(18) Roh, K. H.; Martin, D. C.; Lahann, J. Triphasic Nanocolloids. *J. Am. Chem. Soc.* **2006**, *128*, 6796−6797.
(19) Roh, K. H.; Martin, D. C.; Lahann, J. Biphasic Janus particles with nanoscale anisotropy. *Nat. Mater.* **2005**, *4*, 759−763.
(20) Yuet, K. P.; Hwang, D. K.; Haghgooie, R.; Doyle, P. S. Multifunctional Superparamagnetic Janus Particles. *Langmuir* **2010**, *26*, 4281−4287.
(21) Motoyoshi, K.; Tajima, A.; Higuchi, T.; Yabu, H.; Shimomura, M. Static and Dynamic Control of Phase Separation Structures in Nanoparticles of Polymer Blends. *Soft Matter* **2010**, *6*, 1253−1257.
(22) Landfester, K. Miniemulsion Polymerization and the Structure of Polymer and Hybrid Nanoparticles. *Angew. Chem., Int. Ed.* **2009**, *48*, 4488−4507.
(23) Guo, H.; Qiu, X.; Zhou, J. Self-Assembled Core-Shell and Janus Microphase Separated Structures of Polymer Blends in Aqueous Solution. *J. Chem. Phys.* **2013**, *139*, 084907−084913.
(24) Higuchi, T.; Tajima, A.; Yabu, H.; Shimomura, M. Spontaneous Formation of Polymer Nanoparticles with Iinner Micro-Phase Separation Structures. *Soft Matter* **2008**, *4*, 1302−1305.
(25) Yabu, H.; Higuchi, T.; Shimomura, M. Unique Phase-Separation Structures of Block-Copolymer Nanoparticles. *Adv. Mater.* **2005**, *17*, 2062−2065.

DOI: 10.1021/acs.langmuir.7b00291
Langmuir 2017, 33, 6021−6028

(26) Higuchi, T.; Tajima, A.; Motoyoshi, K.; Yabu, H.; Shimomura, M. Frustrated Phases of Block Copolymers in Nanoparticles. *Angew. Chem.* **2008**, *120*, 8164−8166.
(27) Wurm, F.; Kilbinger, A. Polymeric Janus Particles. *Angew. Chem., Int. Ed.* **2009**, *48*, 8412−8421.
(28) Pawar, A. B.; Kretzschmar, I. Fabrication, Assembly, and Application of Patchy Particles. *Macromol. Rapid Commun.* **2010**, *31*, 150−168.
(29) Johnson, B. K.; Prud'homme, R. K. Chemical Processing and Micromixing in Confined Impinging Jets. *AIChE J.* **2003**, *49*, 2264−2282.
(30) Liu, Y.; Cheng, C.; Liu, Y.; Prud'homme, R. K.; Fox, R. O. Mixing in a multi-inlet vortex mixer (MIVM) for flash nano-precipitation. *Chem. Eng. Sci.* **2008**, *63*, 2829−2842.
(31) Kumar, V.; Wang, L.; Riebe, M.; Tung, H. H.; Prud'homme, R. K. Formulation and Stability of Itraconazole and Odanacatib Nanoparticles: Governing Physical Parameters. *Mol. Pharmaceutics* **2009**, *6*, 1118−1124.
(32) Budijono, S. J.; Russ, B.; Saad, W.; Adamson, R. K.; Prud'homme Block, D. H. Block Copolymer Surface Coverage on Nanoparticles. *Colloids Surf., A* **2010**, *360*, 105−110.
(33) Chen, T.; Hynninen, A. P.; Prud'homme, R. K.; Kevrekidis, I. G.; Panagiotopoulos, A. Z. Coarse-Grained Simulations of Rapid Assembly Kinetics for Polystyrene-b-poly(ethylene oxide) Copolymers in Aqueous Solutions. *J. Phys. Chem. B* **2008**, *112*, 16357−16366.
(34) Spaeth, J. R.; Kevrekidis, I. G.; Panagiotopoulos, A. Z. A Comparison of Implicit- and Explicit-Solvent Simulations of Self-assembly in Block Copolymer and Solute Systems. *J. Chem. Phys.* **2011**, *134*, 164902−164913.
(35) Zhang, C.; Pansare, V. J.; Prud'homme, R. K.; Priestley, R. D. Flash Nanoprecipitation of Polystyrene Nanoparticles. *Soft Matter* **2012**, *8*, 86−93.
(36) Nikoubashman, A.; Lee, V. E.; Sosa, C.; Prud'homme, R. K.; Priestley, R. D.; Panagiotopoulos, A. Z. Directed Assembly of Soft Colloids through Rapid Solvent Exchange. *ACS Nano* **2016**, *10*, 1425−1433.
(37) Sosa, C.; Liu, R.; Tang, C.; Qu, F.; Niu, S.; Bazant, M. Z.; Prud'homme, R. K.; Priestley, R. D. Soft Multifaced and Patchy Colloids by Constrained Volume Self-Assembly. *Macromolecules* **2016**, *49*, 3580−3585.
(38) Lee, V. E.; Sosa, C.; Liu, R.; Prud'homme, R. K.; Priestley, R. D. A Scalable Platform for Structured and Hybrid Soft Nanocolloids by Continuous Precipitation in a Confined Environment.*Langmuir*. [Online early access] DOI: 10.1021/acs.langmuir.7b00249. Published Online: Mar 20, 2017.
(39) Rubinstein, M.; Colby, R. H. *Polymer Physics*; Oxford University Press: New York, 2003.
(40) Bishop, M.; Kalos, M. H.; Frisch, H. L. Molecular Dynamics of Polymeric Systems. *J. Chem. Phys.* **1979**, *70*, 1299−1304.
(41) Grest, G. S.; Kremer, K. Molecular Dynamics Simulation for Polymers in the Presence of a Heat Bath. *Phys. Rev. A: At., Mol., Opt. Phys.* **1986**, *33*, 3628−3631.
(42) Polson, J. M.; Moore, N. Simulation Study of the Coil-globule Transition of a Polymer in Solvent. *J. Chem. Phys.* **2005**, *122*, 024905.
(43) Weeks, J. D.; Chandler, D.; Andersen, H. C. Role of Repulsive Forces in Determining the Equilibrium Structure of Simple Liquids. *J. Chem. Phys.* **1971**, *54*, 5237−5247.
(44) Mandema, W.; Zeldenrust, H. Diffusion of Polystyrene in Tetrahydrofuran. *Polymer* **1977**, *18*, 835−839.
(45) http://codeblue.umich.edu/hoomd-blue.
(46) Anderson, J. A.; Lorenz, C. D.; Travesset, A. General Purpose Molecular Dynamics Simulations Fully Implemented on Graphics Processing Units. *J. Comput. Phys.* **2008**, *227*, 5342−5359.
(47) Torza, S.; Mason, S. G. Three-Phase Interactions in Shear and Electrical Fields. *J. Colloid Interface Sci.* **1970**, *33*, 67−83.
(48) Hobbs, S. Y.; Dekkers, M. E. J.; Watkins, V. H. Effect of Interfacial Forces on Polymer Blend Morphologies. *Polymer* **1988**, *29*, 1598−1602.
(49) Winzor, C. L.; Sundberg, D. C. Conversion Dependent Morphology Predictions for Composite Emulsion Polymers: 2. Artificial Latices. *Polymer* **1992**, *33*, 4269−4279.
(50) Saito, N.; Kagari, Y.; Okubo, M. Effect of Colloidal Stabilizer on the Shape of Polystyrene/Poly(methyl methacrylate) Composite Particles Prepared in Aqueous Medium by the Solvent Evaporation Method. *Langmuir* **2006**, *22*, 9397−9402.
(51) Roh, K. H.; Martin, D. C.; Lahann, J. Biphasic Janus Particles with Nanoscale Anisotropy. *Nat. Mater.* **2005**, *4*, 759−763.
(52) Wang, Y.; Guo, B. H.; Wan, X.; Xu, J.; Wang, X.; Zhang, Y. P. Janus-Like Polymer Particles Prepared via Internal Phase Separation from Emulsified Polymer/Oil Droplets. *Polymer* **2009**, *50*, 3361−3369.
(53) Kirkwood, J. G.; Buff, F. P. The Statistical Mechanical Theory of Surface Tension. *J. Chem. Phys.* **1949**, *17*, 338−343.
(54) Zhou, T.; Chen, S. B. Monte Carlo Simulations of Dendrimer-Polymer Conjugates. *Macromolecules* **2005**, *38*, 8554−8561.
(55) Keßler, S.; Schmid, F.; Drese, K. Modeling Size Controlled Nanoparticle Precipitation with the Co-solvency Method by Spinodal Decomposition. *Soft Matter* **2016**, *12*, 7231−7240.
(56) Beattie, J. K.; Djerdjev, A. M.; Warr, G. G. The Surface of Neat Water is Basic. *Faraday Discuss.* **2009**, *141*, 31−39.
(57) Beattie, J. K.; Djerdjev, A. M.; Gray-Weale, A.; Kallay, N.; Lützenkirchen, J.; Preočanin, T.; Selmani, A. pH and the Surface Tension of Water. *J. Colloid Interface Sci.* **2014**, *422*, 54−57.
(58) Vácha, R.; Rick, S. W.; Jungwirth, P.; de Beer, A. G. F.; de Aguiar, H. B.; Samson, J.-S.; Roke, S. The Orientation and Charge of Water at the Hydrophobic Oil Droplet-Water Interface. *J. Am. Chem. Soc.* **2011**, *133*, 10204−10210.

DOI: 10.1021/acs.langmuir.7b00291
Langmuir 2017, 33, 6021−6028